Progress in Propulsion Physics **8** (2016) 241-262
DOI: 10.1051/eucass/201608241

A WIDE CHARACTERIZATION OF PARAFFIN-BASED FUELS MIXED WITH STYRENE-BASED THERMOPLASTIC POLYMERS FOR HYBRID PROPULSION

M. Boiocchi[1], P. Milova[1], L. Galfetti[1], L. Di Landro[1], and A. K. Golovko[2]

[1]Politecnico di Milano
Aerospace Science and Technology Department
Milano I-20156, Italy

[2]Institute of Petroleum Chemistry
Siberian Branch of the Russian Academy of Sciences
Tomsk, Russia

In the framework of a long-term research activity focused on the development of high-performance solid fuels for hybrid rockets, paraffin-based fuels were investigated and characterized using two different pure paraffinic waxes and a styrene-based thermoplastic elastomer as strengthening material. The fuels were studied using differential scanning calorimetry (DSC) and thermogravimetric analysis / differential thermal analysis (TGA-DTA). The viscosity of the melt layer, responsible for the entrainment effect, was investigated using a Couette viscosimeter. The storage modulus (G') was analyzed using a parallel-plate rheometer. The chemical composition of the pure paraffinic materials was studied using gas chromatography / mass spectrometry (GC-MS), while mechanical properties were investigated through uniaxial tensile tests.

1 INTRODUCTION

Research activities performed at Stanford University at the beginning of the XXI century showed that the surface regression rate of paraffin-based fuels for hybrid rockets is from 3 to 4 times higher than that of conventional hybrid fuels [1–3], such as hydroxyl-terminated polybutadiene (HTPB). For this reason, paraffin-based materials have proved to be very attractive fuels for hybrid rocket propulsion systems. While melting, these fuels form a thin, hydrodynamically unstable liquid layer on the surface and the entrainment of droplets from the

liquid–gas interface increases the rate of fuel mass transfer [4]. The main drawback of paraffin waxes is represented by unsuitable mechanical properties [5]. In order to develop a family of fuels with ballistic and mechanical properties suitable for high-thrust class boosters, two paraffin-based fuels were investigated and characterized using two different pure paraffinic waxes and a styrene-based thermoplastic elastomer as strengthening material. A styrene–ethylene–butylene–styrene block copolymer grafted with maleic anhydride (SEBS-MA) [6–8] was melted and mixed with the paraffin wax under nitrogen atmosphere to prevent oxidative phenomena. The thermal behavior of petroleum waxes (paraffin slack wax) and paraffin-based fuels was studied using DSC and TGA-DTA, which allowed investigating the influence of the different paraffin wax properties. The DSC data show two partially overlapping melting peaks (32–34 and 53–54 °C) and the third extended peak (243–273 °C) linked to the evaporation/pyrolysis of the wax. The viscosity of the melt layer, affecting the entrainment effect, was investigated using a Couette viscosimeter; the storage modulus (G') was analyzed using a parallel-plate rheometer. All the mixtures containing SEBS-MA show a rheological response supposedly affected by the storage time: three weeks of ageing cause an increase in viscosity between 110% and 25% linked with the rotational frequency. The chemical composition of the pure paraffinic materials was studied using GC, which was also applied for the analysis of the strengthened material ageing. Mechanical properties were investigated through uniaxial tensile tests in order to measure the influence of the thermoplastic polymer used.

2 INVESTIGATED MATERIALS

Paraffin waxes are a mixture of hydrocarbons, mainly, normal alkanes. Carbon numbers span approximately in the range between 18 and 45. Paraffins are rather weak and brittle and for this reason, for applications requiring suitable mechanical properties such as the solid fuel of a hybrid rocket engine, they are ill-suited. Research efforts are devoted to develop high performance materials with a greater stiffness and a greater elongation at break.

The first investigated paraffin was a commercial paraffin (GW), supplied by an Italian company, with a DSC melting point of 54.9 °C. The second was a Russian product, available in the framework of a cooperation agreement between Politecnico di Milano and the Institute of Petroleum Chemistry of Tomsk of the Siberian Branch of the Russian Academy of Sciences. Its DSC melting point was measured to be 53.4 °C. SEBS-MA was supplied by Sigma Aldrich. Different compositions were manufactured and characterized, according to the list and the nomenclature of Table 1. The mixing between SEBS and wax was obtained firstly by melting a 50/50 percent mixture under stirring at 120 °C; when the mixture becomes homogeneous, the last part of paraffin has to be added reducing

Table 1 Composition and density of studied pure paraffinic materials and SEBS-based blends

Fuel	Composition	Theoretical density, g/cm^3
GW	Gelly Wax	0.880
RW	Russian Wax	0.890
SEBS	Styrene 30%, Maleic anhydride 2%	0.910
S05G	SEBS 5%, GW 94%, CB 1%	0.886
S10G	SEBS 10%, GW 89%, CB 1%	0.888
S15G	SEBS 15%, GW 84%, CB 1%	0.889
S15R	SEBS 15%, RW 84%, CB 1%	0.889
S20G	SEBS 20%, GW 79%, CB 1%	0.891
S30G	SEBS 30%, GW 69%, CB 1%	0.894

the temperature at 90 °C. The last ingredient to be added is carbon black. A good temperature control during all these operations is strictly needed in order to prevent a dissociation of maleic anhydride contained in SEBS-MA and at the same time to avoid the partial evaporation of the lighter carbon fractions contained into the paraffin wax. For paraffin-based mixtures, it is generally true that the higher the temperature of the melt, the stronger the shrinkage effect of the mixture into the mold during the cooling.

3 THERMAL CHARACTERIZATION

The DSC measurements of the pure waxes and the different mixtures were performed with a TA Instruments model 2010 CE thermal analyzer system. The calibration was performed with an Indium standard according to norms; all the experiments were performed by using nitrogen gas (33 ml/min) as heating/cooling gas and tested at 10 K/min as temperature ramp. All the samples tested were weighed by a Mettler Toledo electronic balance (0.1-milligram accuracy) and the sample mass ranged between 2.4 and 2.7 mg. Thermogravimetric analyses were carried out using a TA Q500 apparatus (mass sample *ca.* 15 mg, alumina crucibles, heating gas for sample: air, gas flow: 60 ml/min, balance protection gas: nitrogen, flow: 40 ml/min, heating ramp: 10 K/min from 20 to 900 °C).

Figure 1 shows the DSC scan of the GW and RW paraffin waxes used throughout this study. The scan shows the heating cycle, for which the lower transition temperature starting at about 28 °C, with a peak at 32 and 36 °C for RW and GW, respectively, corresponds to the premelting solid–solid transition. The higher transition temperature, which is the same for both selected paraffins (peak

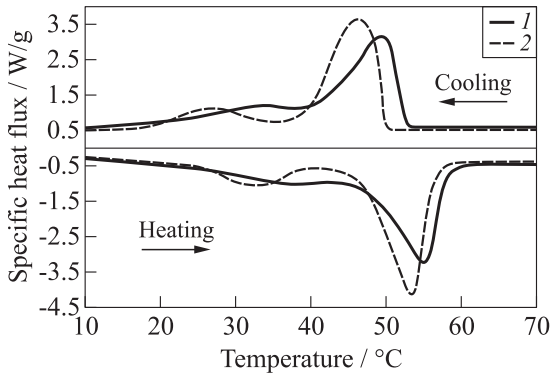

Figure 1 The DSC scans of pure GW (*1*) and RW (*2*) waxes

at 53 °C), is the melting transition temperature. The high-temperature peaks, occurring between 190 and 210 °C, are due to the gasification/decomposition process.

Figure 1 shows the DSC scan of the GW and RW macroparaffin waxes used throughout this study: the endothermic part of the trace shows negative values of specific heat flux. A typical macroparaffin endothermic thermograph is usually composed by two well-defined peaks: the first one (solid–solid transition) is sharper than the second one (solid–liquid transition). Considering the exothermic part of the DSC trace, specular to the endothermic trace, two well-defined peaks can be detected. The main exothermic peak is linked to a liquid–solid transition and it is followed by a sharp peak, showing a solid–solid transition. Considering Fig. 1 and Table 2, a temperature shift of about 5–6 °C can be seen between each endothermic peak and its homologous exothermic peak. This behavior, named supercooling [9], is measured, by definition, by the difference

Table 2 Parameters obtained from DSC measurements for paraffinic waxes

Material	$T_{m,p1}$, °C	$T_{m,p2}$, °C	ΔH_m, J/g	$T_{c,p1}$, °C	$T_{c,p2}$, °C	ΔH_c, J/g
1	2	3	4	5	6	7
GW	39.1	54.9	219.1	33.6	49.5	199.4
RW	32.6	53.4	224.9	26.8	46.2	200.6
S05G	36.7	55.0	224.6	31.0	48.9	207.8
S15G	37.3	55.1	212.5	31.2	48.6	192.9
S30G	37.9	54.7	168.6	32.5	48.7	152.9

Remarks: T — temperature; ΔH — specific enthalpy; m — melting; and c — cooling.

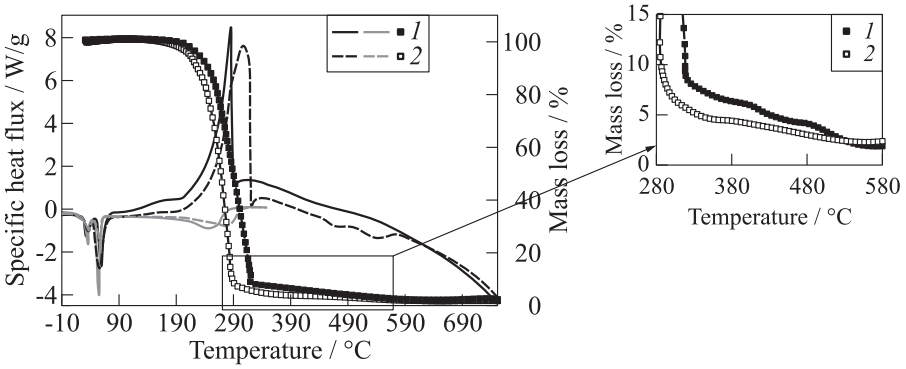

Figure 2 The DSC scans in N_2 and air atmosphere (black curves) overlapped to the TGA curves (grey curves) and mass loss traces for pure paraffinic materials: *1* — GW; and *2* — RW

between the temperature of solid–liquid transition and the temperature of liquid/solid transition. According to [10,11], on heating, some macroparaffin waxes show a transition from an ordered monoclinic crystal structure to a disordered pseudohexagonal crystal rearrangement.

As presented in Fig. 1, GW and RW samples show the typical DSC trace of a macrocrystalline wax with the first solid–solid transition at 39.1 and 32.6 °C, respectively, and, finally, a melting peak at 54.9 and 53.4 °C, respectively. Increasing the temperature of the DSC oven over 200 °C, the thermal behavior of GW and RW (curves *1* and *2*, respectively), is shown in Fig. 2; an endothermic peak between 190 and 300 °C attributed to the gasification/decomposition of the samples can be observed. Considering the blends of GW with SEBS-MA polymer shown in Fig. 3, the absence of the thermal shift of the main endothermic peak is noticed. A similar behavior was observed by Seno and Selvin [12], performing the blends with SEBS-MA and Polyamide12. The measured melting point of GW was 54.9 °C; when the thermoplastic polymer was added (5%, 15%, and 30% mass fraction), the temperature of the minimum of the main peak was between 54.7 and 55.1 °C. This trend is due to the amorphous nature of the polymer or to its very low grade of crystallinity. The DSC trace does not show any relevant endothermic or exothermic peak, as illustrated in Fig. 3 (lines *5*). In a mixture between a paraffinic material and an amorphous material, only the waxy material is detectable by DSC which gives a signal directly proportional to the paraffin mass fraction. Reading the fourth column in Table 2, an inverse proportionality between the values of enthalpy of melting (ΔH_m) and the polymer mass fraction (from 5% to 30%) was observed. In order to understand the thermal behavior of SEBS-MA, a DSC analysis was performed. It was confirmed that SEBS-MA is amorphous; only a negligible peak in the temperature

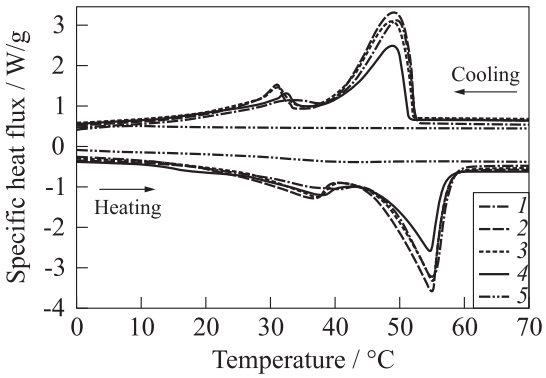

Figure 3 The DSC thermographs of different GW-based formulations with three different SEBS concentrations: *1* — GW; *2* — S05G; *3* — S15G; *4* — S30G; and *5* — SEBS-MA

range 30–50 °C was evidenced which can be attributed to trace of crystallinity of rubber (EB) blocks [13]. Another influence of the polymer content in SEBS-based mixtures detected in DSC thermographs was linked with the temperature of the solid–solid transition peak both in heating and cooling.

As shown in Table 2, a decrease of about 2 °C in heating, compared to GW (39.1 °C), was observed considering S05G and S15G mixtures; S30G shows a decrease of only 1 °C. A specular behavior was detected taking into account the cooling trace.

A comparison in terms of TGA and percentage mass loss curves, for the pure paraffinic materials considered in the present work, is shown in Figs. 2 and 4. A small shift between the second endothermic peak (between 180 and 310 °C) of DSC trace and the TGA exothermic peak is observed in both tested paraffinic waxes. It can be explained considering differences in terms of sensitivity of the apparatus (higher for DSC compared with TGA), sample mass (2 mg for DSC vs. 16 mg for TGA) and setup (inert atmosphere for DSC and oxidative for TGA). A comparison between different TGA curves shows that probably RW (curves *2* in Fig. 2) combustion process is faster than that of the other paraffin samples because of the narrowest exothermic peak. The magnification in Fig. 2 shows the mass loss trends. Observing the final combustion temperature of each sample, different values (289 °C for RW and 320 °C for GW) were obtained because of different chemical species requiring higher temperatures to complete all oxidative reactions.

A similar interpretation can be given considering TGA and mass loss traces of GW and S15G shown in Fig. 4. The magnification of mass loss trace shows that the amount of residuals of S15G at the end of the main combustion process (308 °C) is larger than that of pure GW (19.8% vs. 8.3%). The presence

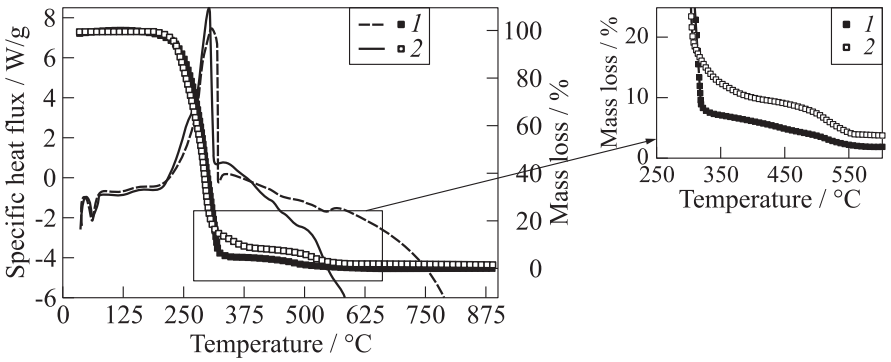

Figure 4 Comparison of the exothermic peaks (curves) and mass loss (curves with signs) for pure GW (*1*) and S15G (*2*)

of 15 %(mass) of SEBS-MA, which is a polymer with a high thermal stability, represents only a part of the possible explanation; some molecules resulting by thermooxidative reactions of the polymer and the paraffin wax react to form carbonaceous products hard to be oxidized.

4 VISCOELASTIC CHARACTERIZATION

In order to obtain the viscoelastic behavior of the investigated formulations, a rotational rheometer was used. All the experiments were carried out by a Rheometrics Dynamic Analyzer RDA II using a Couette apparatus for viscosity measurements on melted materials. This apparatus works in an oven in which an air flux allows to establish a temperature-controlled regime during the test. The outer cylinder rotates, while torque is sensed on the inner nonrotating cylinder. Particular attention must be paid during the pouring of the melted material in order to prevent bubble gas formation. Two samples for each formulation were cut at different sections of the dog-bone samples in order to check the absence of bubbles, confirming the goodness of both manufacturing and pouring procedures used to prepare the samples. A test using this kind of rheological apparatus is usually performed in controlled-rate mode with the shear rate ranging logarithmically between 5 and 1260 s^{-1}. The used test temperature values ranged between 85 and 165 °C.

4.1 Dynamic Viscosity

Figure 5 shows the viscosity behavior of a melted SEBS-based blend (SEBS 15%, Wax 84%, CB 1%) tested at 85 °C, at different rates and in two different

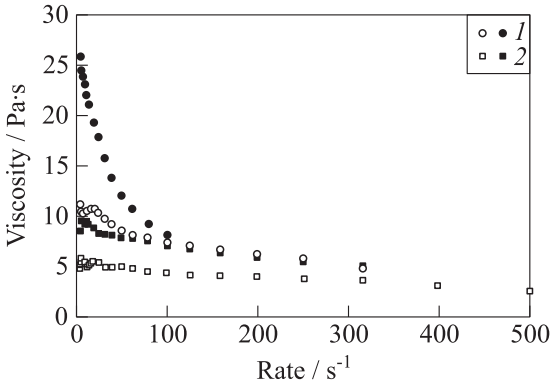

Figure 5 Trend of viscosity for fresh (empty signs) and aged (filled signs) samples of S15G (*1*) and S15R (*2*) at 85 °C

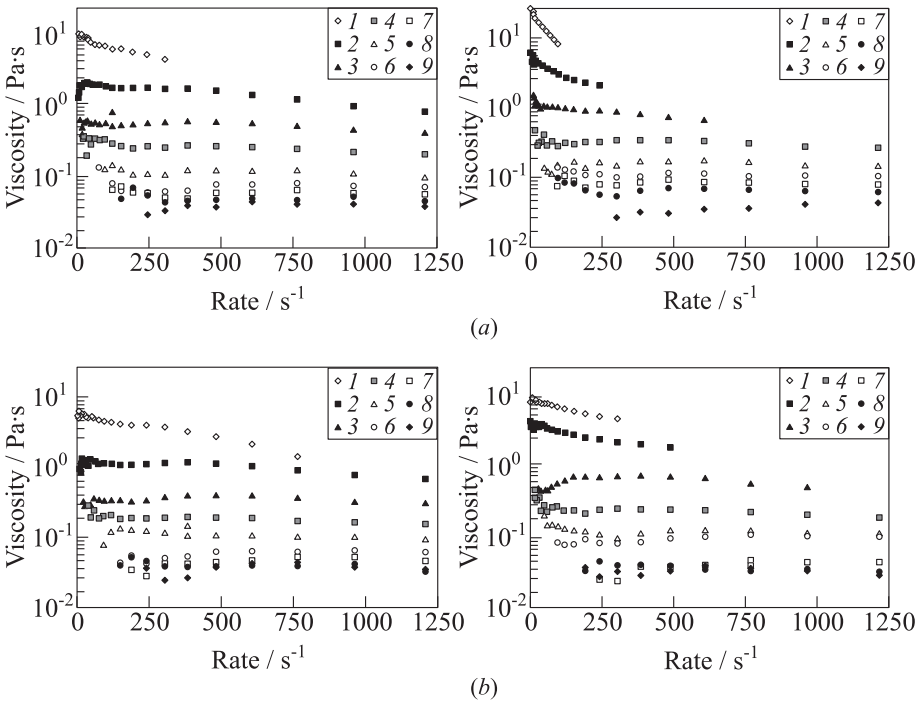

Figure 6 Temperature scans of viscosity for fresh (left column) and aged (right column) samples of S15G (*a*) and S15R (*b*): *1* — 85 °C; *2* — 95; *3* — 105; *4* — 115; *5* — 125; *6* — 135; *7* — 145; *8* — 155; and *9* — 165 °C

Table 3 Viscosity values obtained with Couette rheometer tests at 1000 s^{-1} ordered in decreasing values

Mixture	Temperature, °C							
	95	105	115	125	135	145	155	165
S15G fresh	1.071	0.491	0.236	0.118	0.074	0.059	0.053	0.042
S15G aged	—	—	0.285	0.153	0.106	0.078	0.064	0.041
S15R fresh	0.777	0.327	0.162	0.101	0.064	0.052	0.041	0.038
S15R aged	—	0.508	0.207	0.116	0.105	0.044	0.033	0.034

ageing conditions. The sample S15G (fresh) was tested 24 h after preparation. The same mixture was tested in the same conditions after a three-week storage at 25 °C.

The ageing effect of SEBS-based mixtures containing both GW and RW is shown in Fig. 5. Considering low rates (lower than 100 s^{-1}), the viscosity of aged samples is higher than that of fresh samples for both paraffins. As the rate increases, the viscosity decreases; the RW-based formulation shows a lower viscosity than GW-based formulation. Figure 6 shows the viscosimetric behavior of the same composition (fresh and aged) investigated at a temperature ranging between 85 and 165 °C.

The viscosity of the aged samples is definitely higher than that of the fresh formulations at low temperatures but the gap narrows as the temperature increases. The aged formulation tested at 85, 95, and 105 °C was interrupted (at 100, 250, and 630 s^{-1}, respectively) because the limit of maximum torque was reached. The measured maximum torque values for fresh formulations are always lower than the superimposed limit; for this reason, the graphs were not interrupted in advance.

A comparison between two families of SEBS-based blends containing GW and RW waxes was made; a clear trend was observed. Under the same experimental conditions (temperature of the melt and rate of the Couette apparatus), Table 3 points out that RW-based blends show a lower viscosity than the GW-based mixtures.

Molten blends were tested using a Couette rheometer at different temperatures; extrapolated data at 1000 s^{-1} of shear rate are listed in Table 3, which shows the effects of temperature and ageing on formulations S15G and S15R.

4.2 Rheology

The rheological characterization of thermoplastic polymers and their blends is a complex subject requiring a careful test design. In order to obtain the viscoelastic behavior of the investigated formulations, a rotational rheometer was

used. All experiments were carried out by a Rheometrics Dynamic Analyzer RDA II using a parallel plate apparatus to study the elastic (G') and storage (G'') moduli. This apparatus works in an oven in which an air flux allows to establish a temperature-controlled regime during the test. The lower plate rotates, while torque is sensed on the inner nonrotating plate. Parallel-plate tests were performed considering small amplitude sinusoidal oscillatory testing as function of test frequency. The test temperature values ranged between 19 °C and the melting point, with 3 °C of spacing between each test. The usual range of frequency values in which all the tests were performed was from 0.5 to 50 Hz. All rheological tests were performed using a thin disk (25-millimeter diameter, 1-millimeter thickness) of the material under investigation placing it between the plates of the rheometer and increasing the temperature to obtain a partial melting of the material in direct contact with the metal. The rheological test usually started when the temperature of the sample was stabilized at the room value. This operation was necessary to allow a good physical contact between the plates of the apparatus and the disk of the paraffin-based material under testing.

Figures 7 and 8 show the trend of G' and G'' for pure wax GW and RW, respectively. The shift occurring between the endothermic peak pointed out by DSC test and the beginning of G' sharp decrease (and, symmetrically, the sharp increase of G'') is due to the different mass of the samples (2 mg vs. 2 g). Different masses are characterized by different thermal inertia. A preliminary investigation on the rheological behavior of the selected materials was performed by determining the elastic moduli response by variation of the percentage strain value. A value of percentage strain of 1% was selected as a good trade-off between the needed stress/strain linearity and the sensitivity of the test bench.

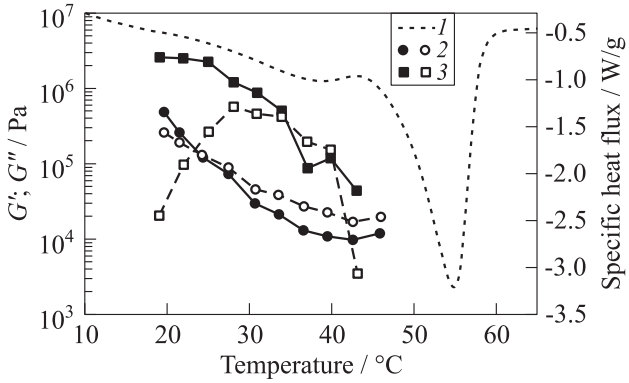

Figure 7 Trend of G' (filled signs) and G'' (empty signs) and specific heat flux (*1*) vs. T for pure wax GW: *2* — strain 1%; and *3* — strain 0.05%

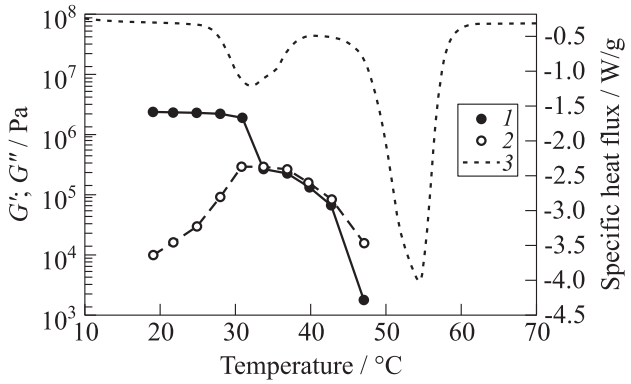

Figure 8 Trend of G' (*1*) and G'' (*2*) and specific heat flux (*3*) vs. T for pure wax RW

The overlapping with DSC traces in Figs. 7 and 8 allows an interpretation of the softening behavior of a typical macrocrystalline paraffin. Figure 7 shows two different sets of G' and G'' traces for GW, obtained working with two strain values: 0.05% and 1%. Only pure GW sample was found to be almost to the stress/strain linearity limit; for this reason, another test with a low percentage strain value was performed: a different behavior was observed. At 1 percent strain, G' and G'' values were found to be very similar along the whole temperature range of test (from 19 to 46 °C), probably, because of the high fragility and softness when compared with RW. Considering G' trace obtained at 0.05% of strain, before 25 °C, the steady behavior of G' was observed, while after 25 °C, a clear decrease in G' values and an increase in G'' were registered. The regular decrease of G' values was ended by the melting of the sample. These two temperatures can be defined as 'critical' and ascribed to the initial part of the solid–solid transition of the paraffinic wax.

If RW in Fig. 8 is considered, a similar behavior of G' and G'' can be observed but in this case, it is possible to detect two critical temperature values. The G' trace before the first critical temperature (31 °C) is characterized by G' values more than one order of magnitude higher than the corresponding G'' values (with a barely noticeable influence of frequency) while after this temperature, G' and G'' values are closer or superimposed. The second critical temperature can be located at 40 °C because after this point, G' values decrease up to the melting of the material. The rheological trace between 31 and 40 °C shows quite stable values of G' and G''. Transition temperature values for pure paraffinic waxes are presented in Table 2 but concerning RW (solid–solid transition 32.6 °C, solid–liquid transition 53.4 °C), a good agreement with the critical temperatures (31 and 40 °C) can be detected. A possible explanation of the presence of two critical temperatures only for RW could be linked with the neat separation (and

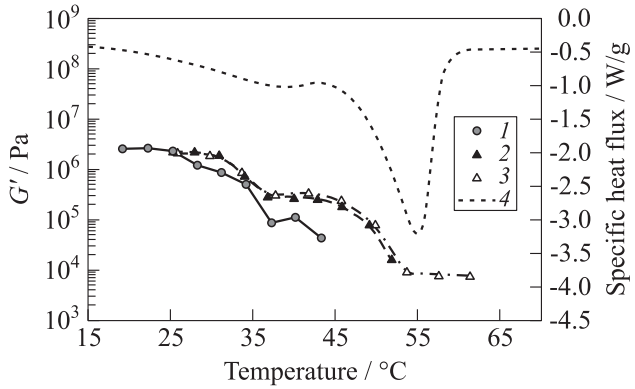

Figure 9 Trend of G' for pure GW (*1*) compared with S15G blend fresh (*2*) and aged (*3*) and specific heat flux of pure GW (*4*)

a strong intensity of the peak) between the solid–solid and solid–liquid transitions which cannot be observed considering GW. A solid–solid transition peak with a slow decrease in heat flux was observed to be linked to a drop in G' modulus values from 12 to 14 °C before reaching the minimum of the endothermic peak as well as observed with GW. The evolution of the crystallinity [10,11] with the temperature shown by DSC trace is linked with an increase of the molecular mobility which is slower for GW compared to RW. This could explain why for GW, the drop of G' values starts at a higher temperature than the one observed studying RW.

The comparison of the relative position of the endothermic peaks given by DSC tests and the behavior of G' and G'' trends for pure GW and fresh S15G allows appreciating how the different phases of GW melting affect G' and G'' behavior. The shift occurring between the endothermic peak pointed out by DSC test and the beginning of G' sharp decrease (and symmetrically, the sharp increase of G'') was, probably, linked to the different mass of the samples (2 mg vs. 2 g) and so to a different thermal inertia. Figure 9 shows the behavior of fresh and aged SEBS-based formulation (SEBS 15%, GW 84%, and CB 1%), in terms of G' and G'', compared with the DSC trace. Two critical temperatures define the G' trace into three main areas. The first one finishes as the solid–solid transition occurs: the G' values are almost constant and frequency-independent. The second can be identified between the solid–solid and the solid–liquid transition of the paraffin: the blend transmits a torque to the rheometer sensor but because of the swelling process, an intense dependence of G' values on percentage strain was observed. The last one can be associated to the temperature range between the solid–liquid transition and a limit temperature (T_{lim}) just before the complete melting of the mixture. For S15G formulations, it occurs immediately

while for S30G, it occurs after about 30 °C. The DSC tests point out that the peak where GW melting occurs is at 54 °C. If the mass fraction of the polymer is larger than 15%, the mixture is liquid at higher temperatures, thus affecting the regression rate behavior. The decrease of the elastic modulus of pure SEBS-MA starts at 80 °C which is close to the limit temperature measured for S30G. Investigations to study structural morphologies [14–20], viscoelastic and thermal properties [21–25] of styrene-based thermoplastic elastomers and their blends with different polymers and fillers were performed. The results show that gels rheological and mechanical properties are affected by block copolymer concentration, molar mass, end/block ratio and chemical compatibility with the filler.

Mechanical properties when SEBS-MA is mixed with polymers (e. g., Nylon 6 or Polyamide 6) have been investigated in order to open the maleic anhydride rings creating stable chemical bonds (or crosslinks). In such cases, SEBS-MA is usually used as impact modifier or compatibilizer [26–29], improving both impact and toughness characteristics. SEBS-MA was chosen after a preliminary experimental investigation about the use of thermoplastic polymers as strengthening materials for paraffin-based formulations. Styrene–isoprene–styrene and SEBS-MA have been studied both from a ballistic and rheological point of view obtaining a clear response indicating the maleated formulation as the best choice. Considering the same experimental conditions (storing temperature, polymer mass fraction, and polystyrene mass fraction), not-maleated polymer-based blends have shown low regression rate and scarce toughness. Figure 10 shows a rheological effect in terms of G' due to the ageing of the SEBS-MA-based blends. Taking into account the viscosimetric characterization of melted mixtures of different paraffin waxes and SEBS-MA, an increase of the maximum temperature, at which the sample can be tested before the melting, was detected after three

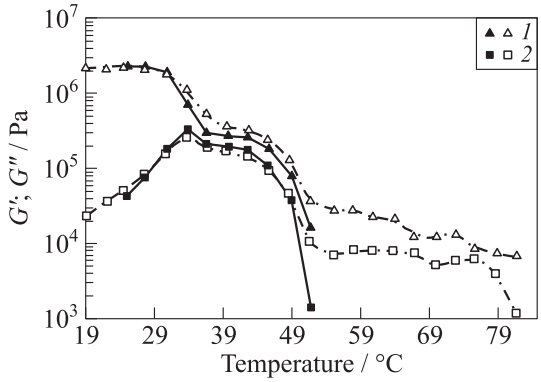

Figure 10 Trend of G' (*1*) and G'' (*2*) for S15G (filled signs) and S30G (empty signs)

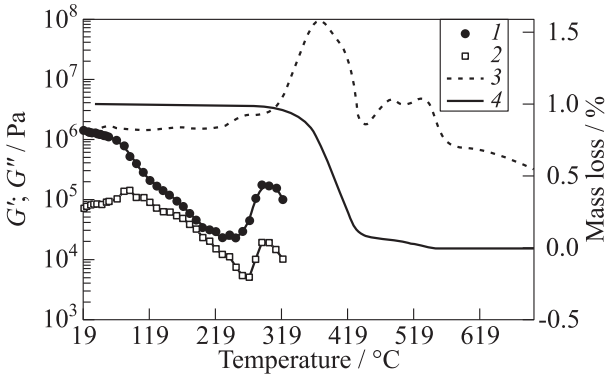

Figure 11 Trend of G' (*1*) and G'' (*2*) for a sample of pure SEBS compared with its TGA trace (*3*); *4* — SEBS mass loss

weeks. Considering the aged S15G sample, T_l was observed to be almost 6 °C higher than that of fresh mixture. The ageing of all the material tested took place at normal conditions without any noticeable changes in temperature (22–23 °C); so, this behavior is likely to be linked with the manufacturing conditions especially with the temperature during the first part of the mixing process. As the temperature of SEBS-MA increases exceeding a limit at which the bond between EB-block and maleic anhydride becomes weak (or unstable), the MA ring is more likely to break.

The SEBS-containing formulations (5%, 15%, and 30%) thermographs seem to be characterized by the same melting temperature of pure GW.

The DSC tests point out that the peak where GW melting occurs is at 54 °C. If the polymer mass fraction is larger than 15%, the mixture is liquid at higher temperatures (G' cannot be measured). This trend negatively affects the regression rate behavior, because of the inhibiting effect on the entrainment phenomenon.

Figure 11 shows the G' and G'' behavior of SEBS tested between 19 and 321 °C. A TGA with a percentage mass loss was reported to correctly identify the start of the sample thermal degradation. The TGA trace indicates that in the range 220–310 °C, a small exothermic peak occurs and it is linked with the final part of the elastic modulus trace. The G' increase is due to the implemented test method and the sample chemical composition. According to the usual method, a sample disk of material (25-millimeter diameter, 1.5-millimeter thickness) was placed in an oven in which it was heated by an air flux. At high temperature, the sample annular surface directly exposed to the air flux undergoes thermooxidative reactions leading to a molecular structure modification of the polymer. Another reason is referred to the maleic anhy-

dride content of the polymer. SEBS-MA is used to increase the mechanical properties of epoxy resins because of the creation of strong chemical bonds between the epoxy ring and the maleic anhydride ring. The maleic anhydride high chemical reactivity at low temperatures explains the small exothermic peak observed.

5 MECHANICAL PROPERTIES

The mechanical characterization was carried out on pure GW and its blends with different amount of SEBS (5%, 10%, 15%, 20%, and 30%) at the speed of 0.5 and 50 mm/min. Material samples were obtained by casting the melted mixture into a mould designed according to UNI-EN-ISO 527 norm for plastic materials. Material testing was performed with a PC-controlled uniaxial tensile test machine equipped with a load cell of 1 kN (Instron Series 4302). Elastic modulus was calculated using both methods (tangent and secant) described in the reference norm: no significant differences occurred.

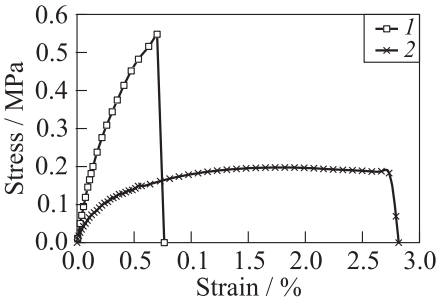

Figure 12 Influence of the temperature on maximum load and elongation at break for pure GW sample at 0.5 mm/min: *1* — 8 °C; and *2* — 21 °C

Figure 12 shows the influence of the temperature of the pure GW samples on maximum load (from 0.54 to 0.2 MPa) and specularly, on the value of elongation at break (which increases from 0.7% to 2.7%). The strong sensitivity to the temperature is linked to the softening of the material starting at 15 °C (see Fig. 1: first soft endothermic peak). Considering SEBS-based samples, as shown in Fig. 13, the higher the polymer fraction is, the higher the elongation at break. Materials with a polymer content lower than 15% (S05G and S10G sample) show a behavior typical for rigid and brittle materials. As the SEBS mass fraction increases, the elongation at break increases with a not linear trend.

A higher content of thermoplastic polymer involves a decrease of the Young Modulus. A more significant decrease of the Young Modulus (51%–63%) is observed when the fuel temperature is higher (here, 8 °C) and a lower decrease (13%–24%) when the temperature is low (−19 °C). The Young Modulus (Fig. 14 and Table 4) values are higher for each formulation when the sample temperature decreases (from 8 to −19 °C).

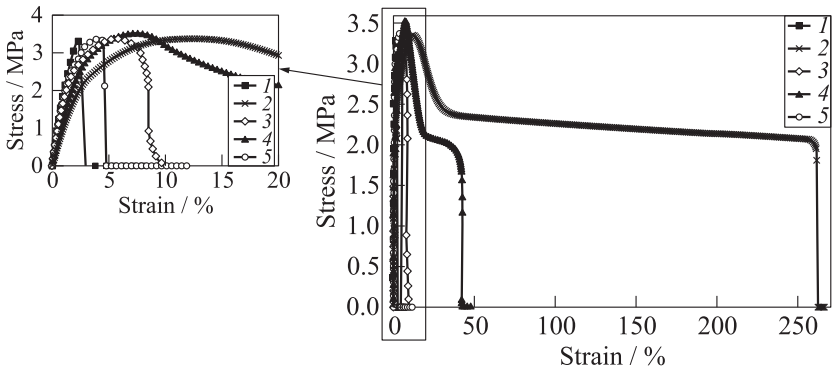

Figure 13 Effects of polymer mass fraction on the elongation at break (T = 8 °C and 50 mm/min): *1* — S05G; *2* — S10G; *3* — S15G; *4* — S20G; and *5* — S30G

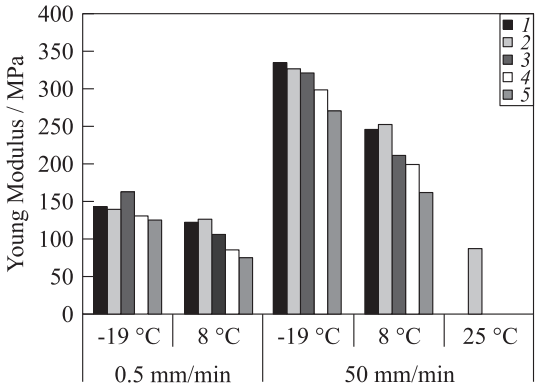

Figure 14 Young Modulus trend of SEBS-based formulations with temperature and elongation speed: *1* — S05G; *2* — S10G; *3* — S15G; *4* — S20G; and *5* — S30G

Table 4 Young Modulus with standard deviation (in MPa) obtained with tensile tests at −19 and 8 °C and 0.5 and 50 mm/min for SEBS-containing formulations

Rate, mm/min	T_{storage}, °C	GW	S05G	S10G	S15G	S20G	S30G
0.5	8	119.2 ± 17.32	123.1 ± 8.0	127.1 ± 1.1	106.7 ± 12.2	86.8 ± 2.1	75.3 ± 5.7
	−19	—	143.1 ± 17.7	141.7 ± 16.1	163.4 ± 12.3	130.6 ± 5.2	126.2 ± 6.5
50	8	—	246.1 ± 23.6	252.8 ± 19.2	211.7 ± 14.6	200.1 ± 4.2	162.6 ± 11.0
	−19	—	334.5 ± 13.9	327.4 ± 36.1	320.7 ± 14.2	299.4 ± 16.6	269.8 ± 2.3

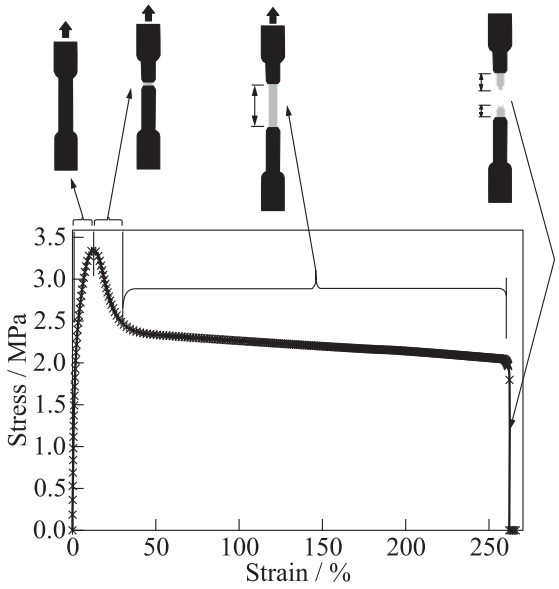

Figure 15 The S30G stress/strain trace divided into four main sections linked with a schematic representation of the dog-bone sample shape evolution

In Fig. 13, S15G shows a stress/strain trace typical of brittle materials: immediately after the achievement of the maximum stress, the break of the dog-bone sample is observed. This is probably due to the polymer low concentration which is not able to change the typical brittle behavior of the paraffin wax. S30G has a quite different behavior showing a ductile stress/strain trace. When the stress reaches the maximum value (3.3 MPa), a change in the mechanical behavior of the material is observed as the sample is not more able to tolerate the stress. When the strain increases, the stress decreases until the break point (at 262 percent strain).

Figure 15 shows how the shape of the dog-bone sample changes with the strain. Four main parts can be observed considering the stress/strain trace and each one is linked to a particular shape of the sample. The first part (0%–12%) shows a linear stress/strain trace, the sample shape is regular, the color is dark. The fast decrease of the stress in the second part (12%–32%) is linked to the appearance of a small striction, the color becomes grey. In the third part, both the length of the striction and the strain grow (32%–260%), until they reach the maximum at the break point. The color of the restriction of the dog bone is grey because of the presence of wax crystals on the sample external surface. This behavior is due to the straightening (deentanglement) of the polymer molecules because of the increase of strain, which involves the

expulsion of wax crystals towards the surface. Considering the low temperature of the sample (8 °C), all the styrenic micelles are cohesive; only the elastomeric midblocks operate.

6 PROPERTIES OF TRADITIONAL HTPB- AND PARAFFIN-BASED FUELS

A comparison of fuel properties measured in this work with mechanical properties of HTPB and thermal and mechanical properties of different paraffin-based fuel formulations is reported in Tables 5 and 6, respectively. The comparison is affected by the composition of the fuel, by different standards and reference values, which strongly can change the measured values. For this reason, the comparison aims to compare the orders of magnitude and to show where improvements are needed for a successful use of paraffin-based fuels in space

Table 5 Mechanical properties of HTPB-based fuels (T_{test} — test temperature; σ_m — maximum stress; ε_m — elongation at maximum stress; E — Young Modulus; and ND — not determined)

Material	T_{test}, °C	σ_m, MPa	ε_m, %	E, MPa	Method	Reference
HTPB R45M	−30	2.0	25.0	24.3	ND	[30]
HTPB R45M	20	0.9	26.0	5.4	ND	[30]
HTPB R45M*	23	0.6–0.9	190–430	0.2–0.5	ND	[31]
HTPB**	23	2.1–21.6	260–480	—	ASTM D412	[32]

*NCO content varying between 4.9% and 9%.

**NCO/OH ranging from 1.0 and 1.2.

Table 6 Mechanical properties of paraffin-based fuels

Material	T_{test}, °C	T_{mp}, °C	σ_m, MPa	ε_m, %	E, MPa	Method	Reference
Wax	—	56–58	1.2	2.3	24.3	ND	[33]
Wax	25	53	0.8	12.0	61.4	ASTM D639-95	[34]
Wax	15	48	170.0	5.3	171.0	ASTM D639-95	[35]
	25	48	80.0	13.1	81.6	ASTM D639-95	[35]
	30	48	42.1	105.3	60.5	ASTM D639-95	[35]
Wax*	—	54–64	0.9–1.0	0.4–0.6	190–260	ASTM D412	[36]
Wax**	—	99–104	4.0–12.5	90–800	100–1000	ASTM D412	[36]
	—	53–55	0.55	up to 260	75–335	UNI-EN-ISO 527	Present work

*Several paraffin wax formulations.

**Low-density polyethylene.

propulsion applications. The measured properties for the formulations studied in this work show that the investigated fuels can compete with traditional HTPB-based fuels and are in good agreement with paraffin-based formulations discussed in the literature. Further research activities could improve the values for σ_m (maximum stress), considering that increase of σ_m leads to a decrease of ε_m (elongation at maximum stress). A balance between these two properties is linked to the specific mission requirements. According to the Young Modulus, the measured values, which are in the range 75–335 MPa, comply with the needs.

On the whole, the investigated formulations show good properties for their use as solid fuels in hybrid propulsion applications.

7 CONCLUDING REMARKS

The paper discusses the characterization results of paraffin-based fuels mixed with a styrene-based thermoplastic elastomer used as strengthening material. The DSC and TGA-DTA techniques, a parallel plate rheometer, a Couette viscosimeter, gas-cromatography, and uniaxial tensile tests were used to characterize pure paraffins and their blends.

The overlapping of DSC thermographs and elastic modulus traces confirms the presence of critical temperature values which explain the rheological behavior of paraffin wax blended with different mass fractions of SEBS-MA.

For GW-based blends such as S15G and S30G, two critical temperatures can be seen dividing G' trace into three main areas. The DSC tests point out that the peak where GW melting occurs is at 54 °C. If the mass fraction of the polymer is larger than 15%, the mixture is liquid at higher temperatures, negatively affecting the regression rate behavior.

The materials with a polymer content lower than 15% (S05G and S10G samples) show a behavior typical for rigid and brittle materials. As the SEBS mass fraction increases, the elongation at break increases with a not linear trend. A higher content of thermoplastic polymer involves a decrease of the Young Modulus. A more significant decrease of the Young Modulus (51%–63%) is observed when the fuel temperature is higher (here, 8 °C) and a lower decrease (13%–24%) when the temperature is low (−19 °C). The Young Modulus values are higher for each formulation when the sample temperature decreases (from 8 to −19 °C).

Considering ageing effects, for the three-week aged S15G sample, the limit temperature (T_l) was almost 6 °C higher than that of the fresh mixture.

On the whole, the formulations investigated in this work show suitable properties for their use as low melting temperature solid fuels in hybrid rockets applications.

REFERENCES

1. Chiaverini, M. J., N. Serin, D. Johnson, Y. C. Lu, K. K. Kuo, and G. A. Risha. 2000. Regression rate behavior of hybrid rocket solid fuels. *J. Propul. Power* 16(1):125–132.
2. Karabeyoglu, M. A., B. J. Cantwell, and D. Altman. 2001. Development and testing of paraffin-based hybrid rocket fuels. AIAA Paper No. 2001-4503.
3. Karabeyoglu, M. A., G. Zilliac, B. J. Cantwell, S. DeZilwa, and P. Castellucci. 2004. Scale-up tests of high regression rate paraffin-based hybrid rocket fuels. *J. Propul. Power* 20(6):1037–1045.
4. Karabeyoglu, M. A., and B. J. Cantwell. 2002. Combustion of liquefying hybrid propellants: Part 2. Stability of liquid films. *J. Propul. Power* 18(3):621–630.
5. Maruyama, S., T. Ishiguro, K. Shinohara, and I. Nakagawa. 2011. Study on mechanical characteristics of paraffin-based fuel. *47th AIAA/ASME/SAE/ASEE Joint Propulsion Conference & Exhibit*. San Diego, CA.
6. Prasman, E. 1997. Morphology and mechanical behavior of oriented blends of styrene–isoprene–styrene triblock copolymer and mineral oil. Massachussetts Institute of Technology. Master Thesis.
7. Kim, J. K., M. A. Paglicawan, and M. Balasubramanian. 2006. Viscoelastic and gelation studies of SEBS thermoplastic elastomer in different hydrocarbon oils. *Macromol. Res.* 14(3):365–372.
8. Zhang, Q., S. Song, J. Feng, and P. Wu. 2012. A new strategy to prepare polymer composites with versatile shape memory properties. *J. Mater. Chem.* 22:24776.
9. Royon, L., and G. Guiffant. 2001. Heat transfer in paraffin oil/water emulsion involving supercooling phenomenon. *Energ. Convers. Manage.* 42:2155–2161.
10. Chazhengina, S. Y., E. N. Kotelnikova, I. V. Filippova, and S. K. Filatov. 2003. Phase transition of n-alkanes as rotator crystals. *J. Mol. Struct.* 647:243.
11. Alcazar-Vara, L. A., and E. Buenrostro-Gonzalez. 2013. Liquid–solid phase equilibria of paraffinic systems by DSC measurements. *Applications of calorimetry in a wide context — differential scanning calorimetry, isothermal titration calorimetry and microcalorimetry*. Ed. A. A. Elkordy. InTech. Ch. 11. 253–276. doi: 10.5772/54575.
12. Seno, J., and T. P. Selvin. 2006. Thermal and crystallisation behaviours of blends of polyamide 12 with styrene–ethylene/butylene styrene rubbers. *Polymer* 47:6328–6336.
13. Zheng, M., and W. Du. 2006. Phase behavior, conformations, thermodynamic properties, and molecular motion of multicomponent paraffin waxes: A raman spectroscopy study. *Vib. Spectrosc.* 40:219–224.
14. Reynders, K., N. Mishenko, and K. Mortensen. 1995. Stretching-induced correlations in triblock copolymer gels as observed by small-angle scattering. *Macromolecules* 28:8699.
15. Laurer, J. H., R. Bukovnik, and R. J. Spontak. 1996. Morphological characteristics of SEBS thermoplastic elastomer gels. *Macromolecules* 29:5760.

16. Kleppinger, R., M. van Es, N. Mishenko, M. H. J. Koch, and H. Reynaers. 1998. Physical gelation in a triblock copolymer solution: *In situ* study of stress–strain behavior and structural development. *Macromolecules* 31:5805.

17. Kleppinger, R., N. Mishenko, H. Reynaers, and M. H. J. Koch. 1999. Long-range order in physical networks of gel-forming triblock copolymer solutions. *J. Polym. Sci. Pol. Phys.* B37:1833.

18. Wilkinson, A. N., M. L. Laugel, V. M. Clemens, V. M. Harding, and M. Marin. 1999. Phase structure in polypropylene/PA6/SEBS blends. *Polymer* 40:4971–4975.

19. Asthana, S., and J. P. Kennedy. 2002. Novel polyisobutylene stars. XXIII. Thermal, mechanical and processing characteristics of poly(phenylene ether)/polydivinylbenzene(polyisobutylene-b-polystyrene)$_{37}$ blends. *J. Appl. Polym. Sci.* 86:2866–2872.

20. Litmanovich, A. D., N. A. Platé, and Y. V. Kudryavtsev. 2002. Reactions in polymer blends: Interchain effects and theoretical problems. *Prog. Polym. Sci.* 27:915–970.

21. Laurer, J. H., J. Mulling, S. A. Khan, R. Spontak, and R. Bukovnik. 1998. Thermoplastic elastomer gels. I. Effects of composition and processing on morphology and gel behavior. *J. Polym. Sci. Pol. Phys.* B36(13):2379.

22. Laurer, J. H., J. Mulling, S. A. Khan, R. Spontak, and R. Bukovnik. 1998. Thermoplastic elastomer gels. II. Effects of composition and temperature on morphology and gel rheology. *J. Polym. Sci. Pol. Phys.* B36(14):2513–2523.

23. Dezhen, W., X. Wang, and R. Jin. 2004. Toughening of poly(2,6-dimethyl-1,4-phenylene oxide)/nylon 6 alloys with functionalized elastomers via reactive compatibilization: Morphology, mechanical properties and rheology. *Eur. Polym. J.* 40:1223–1232.

24. Wang, J., M. D. Calhoun, and S. J. Severtson. 2008. Dynamic rheological study of paraffin wax and its organoclay nanocomposites. *J. Appl. Polym. Sci.* 108:2564–2570.

25. Pracella, M., M. Haque, and V. Alvarez. 2010. Functionalization, compatibilization and properties of polyolefin composites with natural fibers. *Polymers* 2:554–574.

26. Horiuchi, S., N. Matchariyakul, K. Yase, and T. Kitano. 1997. Compatibilizing effect of maleic anhydride functionalized SEBS triblock elastomer through a reaction induced phase formation in the blends of polyamide6 and polycarbonate: 2. Mechanical properties. *Polymer* 38(1):59–78.

27. Wilkinson, A. N., M. L. Clemens, and V. M. Harding. 2004. The effect of SEBS-g-maleic anhydride reaction on the morphology and properties of polypropylene/PA6/SEBS ternary blends. *Polymer* 45:5239–5249.

28. Huang, J. J., H. Keskkula, and D. R. Paul. 2006. Elastomer particle morphology in ternary blends of maleated and non-maleated ethylene-based elastomers with polyamides: Role of elastomer phase miscibility. *Polymer* 47:639–651.

29. Chow, W. S., Y. Y. Leu, and Z. A. Mohd Ishak. 2012. Effects of SEBS-g-MAH on the properties of injection moulded poly(lactic acid)/nano-calcium carbonate composites. *Express Polym. Lett.* 6(6):503–510.

30. Maruizumi, H., K. Kosaka, S. Suzuki, and D. Fukuma. 1988. Development of HTPB binder for solid propellants. AIAA Paper No. 88-3352.

31. Haska, S., E. Bayramli, F. Pekel, and S. Ozkar. 1996. Mechanical properties of HTPB-IPDI-based propellants. *J. Appl. Polym. Sci.* 64:2347–2354.

32. Vilar, W., and L. Akcelrud. 1995. Effect of HTPB structure on prepolymer characteristics and on mechanical properties of polybutadiene-based polyurethanes. *Polym. Bull.* 35:635–639.

33. Asadchii, O. G., B. Z. Votlokhin, N. F. Bogdanov, and V. P. Gladyshev. 1979. Determination of tensile strength of paraffin waxes. *Khimiya i Tekhnologiya Topliv i Masel* 10:51–53.

34. Wang, J., S. J. Severtson, and A. Stein. 2006. Significant and concurrent enhancement of stiffness, strength, and toughness for paraffin wax through organoclay addition. *Adv. Mater.* 18:1585–1588.

35. Pu, G., J. Wang, and S. J. Severtson. 2007. Properties of paraffin wax/montmorillonite nanocomposite coatings. *NSTI Nanotechnology Conference and Trade Show Technical Proceedings*. Santa Clara, CA. 2:112–115.

36. DeSain, J. D., B. B. Brady, K. M. Metzler, T. J. Curtiss, and T. V. Albright. 2009. Tensile tests of paraffin wax for hybrid rocket fuel grains. AIAA Paper No. 2009-5115.